DOE/ET-53088-84 IFSR #84

KINETIC THEORY OF ALFVEN WAVES

S. M. Mahajan
Fusion Research Center
Institute for Fusion Studies
University of Texas
Austin, Texas 78712

March 1983

Kinetic Theory of Shear Alfvén Waves

by

S. M. Mahajan

Fusion Research Center
Institute for Fusion Studies
University of Texas
Austin, Texas 78712

Abstract

The addition of electron parallel dynamics in the description of an inhomogeneous current carrying cylindrical plasma is shown to replace the magnetohydrodynamic continuum, associated with Alfvén waves, by a discrete spectrum. The spectrum of the resulting discrete modes is determined analytically and numerically.

I. Introduction

In a magnetohydrodynamic (MHD) description of an inhomogeneous plasma, the shear Alfvén wave is the solution of a second order singular differential equation, and is therefore characterized by a continuous spectrum.[1-2] The singularity is at $\omega^2 = k_\parallel^2(r)v_A^2(r)$, where ω is the wave frequency, $k_\parallel$ is the wave number in the direction of the ambient magnetic field $\underset{\sim}{B}_0$, $v_A = B_0/((4\pi\rho)^{1/2}$ is the Alfvén speed, ρ the plasma density, and r is the direction of inhomogeneity. It is expected that a more realistic treatment of the plasma should result in a nonsingular system with discrete eigenmodes of the shear Alfvén wave as its solutions. Rosenbluth and Rutherford[3] attempted to remove the singularity by introducing first order ion gyroradius effects. Connors, Tang and Taylor[4] recently showed that the inclusion of ion gyroradius to all orders does not result in a discrete spectrum. Drake and Kleva[5] have also studied collisional shear Alfvén waves with particular emphasis on its relationship with the tearing mode theory. Both of these analyses deal with a special case of the modes localized around the mode rational surface, $k_\parallel = 0$, in a sheared slab, and obtain a spectrum by introducing dissipation (collisional or kinetic). This variety of modes is important for stability consideration, ($k_\parallel = 0$ are the most unstable perturbations) and is characterized by very low frequency which is either zero or equals the electron diamagnetic drift frequency ω_{e*}. Such modes, which are a small subclass of Alfvén modes, are not of interest from the heating point of view, becuse they are characterized by low impedances. Thus in order to deal with the problem of plasma heating, we need to study the Alfvén waves with arbitrary $k_\parallel$.

In this paper, we deal with Alfvén waves with arbitrary $k_\parallel$ in an inhomogeneous current carrying plasma with finite ω/ω_{ci} effects in cylindrical geometry ($\omega_{ci} = eB_0/m_i c$ is the cyclotron frequency), and show that the inclusion of parallel electron dynamics (or equivalently retaining the electron inertia) does indeed remove the MHD singularity by adding a fourth order derivative to the mode equation. The resulting discrete spectrum is analytically and numerically investigated.

We remind the reader that the presence of equilibrium currents and finite ω/ω_{ci} effects together with cylindrical curvature is known to lead to the discrete spectrum of Global Alfvén Eigenmodes[6-8] (GAE) below the MHD continuum, that is, the eigenfrequency ω is less than the minimum of $k_\parallel v_A$ in the plasma. Without dissipation, these modes have an accumulation point at the lower edge of the continuum.[7-10] We show here that the inclusion of dissipation results not only in discretizing the canonical MHD continuum but unifies the two discrete spectra; below and above the erstwhile continuum boundary. Needless to say that the boundary of the continuum ceases to be an accumulation point for the global Alfvén eigenmodes. The determination of the mode frequencies, the real as well as the imaginary part, is also important for optimizing the efficiency of plasma heating and current drive using Alfvén waves.

In Sec. II of the paper, we derive the general fourth order equation describing Alfvén waves in an inhomogeneous current carrying kinetic plasma. In Sec. III, we expand the system about the minimum of $k_\parallel^2 v_A^2$, and then Fourier transform to obtain the eigenmode equation. In Sec. IV, we discuss the general features of the equivalent

Schrödinger-like equation, and show that it allows a discrete spectrum. In Sec. V, we derive approximate analytic dispersion relations, and compare them with the results obtained by a numerical integration of the mode equation. Parametric studies of the dispersion relation are also presented. Section VI is devoted to a discussion, and conclusions.

II. Basic Equation

Our derivation of the basic equation closely follows the approach of Ref. 6, which deals with the properties of Alfvén waves in a large aspect ratio, low β, tokamak plasma in cylindrical geometry. We begin with the zero ion temperature limit of the radial and perpendicular components of Ampere's law (perpendicular here means the direction on the magnetic surface which is perpendicular to the field line)

$$(F - k_\perp^2)E_r = i\left[\frac{k_\perp}{r}\frac{d}{dr}\,r - (S+A)\right]E_\perp + ik_\parallel E_\parallel + i\,\frac{(r\delta)'}{r}\,k_\perp E_\perp \,, \tag{1}$$

and

$$\left(F + \frac{d}{dr}\frac{1}{r}\frac{d}{dr}\,r\right)E_\perp = i\left(\frac{d}{dr}\,k_\perp + S+A\right)E_r$$

$$- k_\parallel k_\perp E_\parallel - 2\delta' E_\parallel' + \frac{\delta}{r^2}\,E_\parallel - \frac{(r\delta')'}{r}\,E_\parallel \,, \tag{2}$$

where E_r, $E_\perp$ and $E_\parallel$ are respectively the radial, perpendicular and parallel components of the wave electric field, the prime ($'$) denotes differentiation with respect to r, and

$$F = \alpha_1 \frac{\omega^2}{v_A^2} - k_\parallel^2 \,, \tag{3}$$

with $\alpha_1 = (1 - \omega^2/\omega_{ci}^2)^{-1}$ and $S = (\alpha_1\omega^2/v_A^2)\ (\omega/\omega_{ci})$ representing finite ω/ω_{ci} effects, and

$$A = \frac{1}{r(1+\delta^2)} \left(-2k_{\parallel}\delta + k_{\perp}\delta^2\right) \tag{4}$$

is due to the presence of the parallel current in the plasma. The parallel current produces a poloidal magnetic field B_p, and manifests itself through $\delta \simeq B_p/B_0 = r/Rq \ll 1$, where q is the safety factor. The parallel current also modifies the wavenumbers, which are defined by

$$(1+\delta^2)^{1/2}k_{\parallel} = -\frac{\ell}{R} + \frac{m}{qR} = -\frac{\ell}{R} + \frac{m}{r}\,\delta\,, \tag{5}$$

$$(1+\delta^2)^{1/2}k_{\perp} = \frac{m}{r} - \frac{\ell}{R}\,\delta \tag{6}$$

where ℓ and m are the toroidal and poloidal numbers respectively.

Notice that in Eqs. (1) and (2), we have retained only the leading terms containing $E_{\parallel}$. This is justified because the parallel electric field for Alfvén waves is much smaller than the perpendicular fields $E_{\perp}$ and E_r. We can readily eliminate E_r between Eqs. (1) and (2) to obtain a rather complicated equation relating $E_{\perp}$ and $E_{\parallel}$. Considerable simplification is achieved by assuming that $\omega/\omega_{ci} \sim \delta \ll 1$, and $k_{\perp}^2 \simeq m^2/r^2 > k_{\parallel}^2 \sim \omega^2/v_A^2$, and retaining terms only to $O(\delta)$. Neither of these assumptions is particularly restrictive. Within the context of the above mentioned approximations, we can derive a relatively simple equation [see Appendix A]

$$\left[F - \frac{d}{dr}\frac{F}{rk_\perp^2}\frac{d}{dr}\,r\right]E_\perp + gE_\perp = \frac{k_\parallel}{rk_\perp}\left[\frac{d}{dr}\,r\,\frac{dE_\parallel}{dr} - rk_\perp^2 E_\parallel\right] , \tag{7}$$

where

$$g = \frac{(S+A)'}{k_\perp} + \frac{(S+A)^2}{k_\perp^2} , \tag{8}$$

represents the combined effect of equilibrium current and finite ω/ω_{ci}. It is shown in Ref. 8 that, in Tokamak ordering, the first term on the right-hand side of Eq. (8) is dominant. This term depends on the gradients of current and density.

We would like to point out here that if $E_\parallel$ is neglected, Eq. (7) becomes the standard MHD equation, with F=0 as its singular point leading to the well-known continuum.[1-2] This equation has been extensively studied. With $E_\parallel$ included, we need one more equation relating $E_\perp$ and $E_\parallel$ to complete the system. For this purpose, we could use either the parallel component of Ampere's law, or the quasineutrality condition $\underset{\sim}{\nabla} \cdot \underset{\sim}{J} = 0$, where $\underset{\sim}{J}$ is the perturbed current. In this paper, we use the latter condition, which is [see Ref. 6]

$$ik_\parallel \frac{\zeta}{k_\parallel^2\rho_s^2} E_\parallel + \frac{v_A^2}{r}\frac{d}{dr}\frac{r}{v_A^2}\left(E_r + i\frac{\omega}{\omega_{ci}}E_\perp\right)$$

$$+ ik_\perp\left(E_\perp - i\frac{\omega}{\omega_{ci}}E_r\right) = 0 \quad , \tag{9}$$

where $\rho_s = c_s/\omega_{ci} = (T_e/m_i)^{1/2}/\omega_{ci}$ is the ion gyroradius with electron temperature T_e. For all cases of interest in this study, $k_\parallel^2\rho_s^2 << 1$ implying that the parallel wave length of the mode is much larger than the effective gyroradius.

In Eq. (9), ζ is the collisionless parallel electron response,

$$\zeta = 1 + \frac{\omega}{|k_\parallel|v_e} Z\left(\frac{\omega}{|k_\parallel|v_e}\right) , \tag{10}$$

where Z is the plasma dispersion function, and $v_e = (2T_e/m_e)^{1/2}$ is the electron thermal speed. For most Tokamak plasmas of interest, the collisionless assumption for Alfvén waves is quite valid. For small ℓ and m numbers, the typical wave frequency $\omega \sim 10^7 >> \nu \sim 10^5$, where ν is the collision frequency. However, it is quite straightforward to calculate parallel electron response using a particle conserving Krook collisional operator. The resulting expression for ζ is

$$\zeta = \frac{1 + \frac{\omega+i\nu}{|k_\parallel|v_e} Z\left(\frac{\omega+i\nu}{|k_\parallel|v_e}\right)}{1 + \frac{i\nu}{|k_\parallel|v_e} Z\left(\frac{\omega+i\nu}{|k_\parallel|v_e}\right)} , \tag{11}$$

which reduces to Eq. (10) for ν=0. Thus making use of Eq. (11) for ζ allows us to deal with a collisional plasma as well. Note that in deriving Eq. (11), we have neglected the effects of the parallel current, which will doppler shift ω to $\omega - k_\parallel v_d$, where v_d is the electron drift speed. This is justified because $\omega \simeq k_\parallel/v_A >> k_\parallel v_d$, because $v_d << v_A$. The effect can be retained without complicating the analysis. We would like to point out that in the strongly collisional

limit ($\nu \gg \omega, |k_\parallel| v_e$), Eqs. (9) and (11) simply reduce to one of the equations of resistive magnetohydrodynamics; the temperature dependence in ρ_s^2 exactly cancels the temperature dependence in the expanded Z-functions.

To eliminate E_r between Eqs. (1) and (9), we first rewrite Eq. (1) in the approximate form ($F \ll k_\perp^2$),

$$E_r \simeq -i\left[\frac{1}{rk_\perp}\frac{d}{dr}\, r - \frac{1}{k_\perp^2}(S+A)\right]E_\perp - i\,\frac{k_\parallel}{k_\perp^2}\,E'_\parallel - i\,\frac{(r\delta)'}{rk_\perp}\,E_\parallel\,, \quad (12)$$

and then substitute Eq. (12) into Eq. (9) to yield

$$k_\parallel \frac{\zeta}{k_\parallel^2\rho_s^2}E_\parallel - \frac{1}{r}\frac{d}{dr}\, r\left[\frac{k_\parallel}{k_\perp^2}E'_\parallel + \frac{(r\delta)'}{rk_\perp}E_\parallel\right] = \frac{1}{rk_\perp}\left[\frac{1}{r}\frac{d}{dr}\, r\,\frac{d}{dr}\, r - k_\perp^2\right]E_\perp \quad (13)$$

where only the leading order terms have been retained on the right-hand side. Since $E_\parallel$ is small, it is sufficient to determine it to leading order. On the left side of Eq. (13), the terms in the square brackets are small compared to the first term because $d/dr \sim k_\perp$, $\zeta \sim 1$, and $k_\parallel^2\rho_s^2 \ll 1$. Therefore, Eq. (13) simplifies to

$$E_\parallel \simeq \frac{k_\parallel}{k_\perp}\frac{\rho_s^2}{\zeta}\left[\frac{1}{r^2}\frac{d}{dr}\, r\,\frac{d}{dr}\, r - k_\perp^2\right]E_\perp\,, \quad (14)$$

and, when substituted into Eq. (7), it gives the required fourth order equation

$$\left(F - \frac{d}{dr}\frac{F}{rk_\perp^2}\frac{d}{dr}r\right)E_\perp + gE_\perp$$

$$= \frac{k_\parallel}{rk_\perp}\left[\frac{d}{dr}r\frac{d}{dr} - rk_\perp^2\right]\frac{k_\parallel}{k_\perp}\frac{\rho_s^2}{\zeta}\left(\frac{1}{r^2}\frac{d}{dr}r\frac{d}{dr}r - k_\perp^2\right)E_\perp \qquad (15)$$

which describes Alfvén waves in an inhomogeneous, current carrying, cylindrical plasma. Notice that due to the presence of the fourth order term F=0 is no more a singular point of the differential equation. It must also be stated that Eq. (15) is relatively exact; the only approximations made are $k_\perp^2 > k_\parallel^2 \sim \omega^2/v_A^2$, and the smallness of $k_\parallel^2\rho_s^2$, which automatically guarantees $E_\parallel/E_\perp \ll 1$ [see Eq. [14], and this former condition $\omega \sim k_\parallel v_A(F\simeq 0)$ is generally the domain of the shear Alfvén wave. However, the effects of compression have not been neglected in deriving Eq. (15). In fact, in an inhomogeneous plasma, the shear and the compressional modes are coupled, and an adequate description of Alfvén waves requires the presence of both the polarizations.[7] If $\omega \sim k_\parallel v_A$, then the compressional wave is evanescent with the WKB dispersion relation $k_r^2 + k_\perp^2 = 0$.[6,8-9] Thus the Alfvén waves, even in this frequency range, are some linear combination of the two modes of the homogeneous plasma; the shear and the compressional, and Eq. (15) correctly describes the situation. In the remainder of the paper, we use Alfvén waves in preference to shear Alfvén waves.

We end this section by remarking that Eq. (15) can be used to study the tearing modes in a current carrying compressible plasma.

III. Eigenmode Equation

We are interested in investigating the nature of Alfvén waves in the frequency range given by $F \simeq 0$ or $\omega \simeq k_{\parallel} v_A$. It is clear that $F=0$ is no more a singular point of the differential equation implying that the logarithmically singular solutions, which constitute the MHD continuum, are no more there. For general temperature, current, and density profiles, Eq. (15) should be solved numerically. Most of the important and interesting features of this system, however, can be illustrated by studying the system where the profile of $k_{\parallel}^2 v_A^2$ has a minimum at a point $r=r_0 \neq 0$ in the plasma. Thus, the analysis excludes the cases for which $k_{\parallel}^2 v_A^2$ has a minimum at $r=0$, the plasma center. However, we expect all the general results to be essentially valid even for this case.

Since the modes of interest are characterized by $F \simeq 0$, we carefully expand F around the point r_0, the minimum of $k_{\parallel}^2 v_A^2$, i.e.,

$$\left(k_{\parallel}^2 v_A^2\right)'_{r_0} = 0 \ , \tag{16}$$

because F is a rapidly varying function in the vicinity of r_0. All other quantities in the differential Eq. (15) will be evaluated at $r=r_0$. Within the context of the preceding discussion, it is straightforward to show that Eq. (15) can be cast in the form [see Appendix B for details]

$$\frac{d}{dy}(y^2-\mu)\frac{dE_\perp}{dy} - k_\perp^2 a^2 (y^2-\mu)E_\perp + g_0 E_\perp = \bar{\sigma}\left(\frac{d^2}{dy^2} - k_\perp^2 a^2\right)^2 E_\perp \ , \tag{17}$$

where the new variable y is displaced from $r-r_0$, and is given by

$$y = \frac{r-r_0}{a} + \frac{F_0}{2\Lambda^2}\frac{a}{L_n}$$

where a is the radius of the cylinder, $F_0 = F(r=r_0)$, $L_n^{-1} = (n^{-1}dn/dr)_{r=r_0}$, the density gradient scale length at $r=r_0$, $\Lambda^2 = -(a^2/2)(F'')_{r=r_0}$ and

$$\mu = \frac{F_0}{\Lambda^2}\left[1 + \frac{1}{4}\frac{F_0}{\Lambda^2}\frac{a^2}{L_n^2}\right] \tag{18}$$

is the effective eigenvalue to be determined. In the rest of this paper, all quantities, unless otherwise stated are to be evaluated at $r=r_0$. It is shown in Appendix B, that for modes under consideration $F_0/\Lambda^2 \ll 1$, making $\mu \simeq F_0/\Lambda^2$, and $y \simeq (r-r_0)/a$. In Eq. (17), $k_\perp = (k_\perp)r=r_0 = m/r_0$ is the poloidal mode number, $g_0 = (k_\perp^2 a^2/\Lambda^2)(g)r=r_0$, and

$$\bar{\sigma} = \left(\frac{k_\parallel^2}{\Lambda^2}\frac{\rho_s^2}{a^2}\frac{1}{\zeta}\right)_{r=r_0} \tag{19}$$

is the measure of the non MHD effects; in this case the effect of electron parallel dynamics. Notice that σ will be generally complex. For $\sigma=0$, Eq. (17) reduces to the extensively studied MHD equation with ω/ω_{ci} effects, etc. In this case, it is clear that for $\mu>0$ ($F_0>0$) the equation is singular, and leads to the MHD continuum. For $\mu<0$, however, there is no singularity, and the discrete spectrum of marginally stable global Alfvén waves emerges.[8] With the inclusion of

the non MHD effects ($\bar{\sigma}\neq 0$), the picture changes, and a new discrete spectrum encompassing the continuum and the GAE results.

Equation (17) is best analyzed in the Fourier space. Defining

$$E = \frac{1}{(2\pi)^{1/2}} \int_{-\infty}^{+\infty} dy\ E_\perp \exp(iyp) \ ,$$

$$E_\perp = \frac{1}{(2\pi)^{1/2}} \int_{-\infty}^{+\infty} dp\ E \exp(-iyp) \ , \tag{20}$$

we obtain

$$\frac{d}{dp}\left(p^2+k_\perp^2a^2\right)\frac{dE}{dp} + \left[\mu\left(p^2+k_\perp^2a^2\right) + g_0-\sigma\left(p^2+k_\perp^2a^2\right)^2\right]E = 0 \ ,$$

which becomes

$$\frac{d}{dx}\left(1+x^2\right)\frac{dE}{dx} + \left[\varepsilon\left(1+x^2\right) + g_0-\sigma\left(1+x^2\right)\right]E = 0 \tag{21}$$

where $\varepsilon = k_\perp^2a^2\mu$, $\sigma = k_\perp^4a^4\bar{\sigma}$, and $p = k_\perp ax$. We can further transform Eq. (21) using a new dependent variable

$$\psi = \left(1+x^2\right)^{1/2} E \ , \tag{22}$$

to yield the Schrödinger equation

$$\frac{d^2\psi}{dx^2} + \left[\varepsilon-V(x)\right]\psi = 0 \ , \tag{23}$$

where $\varepsilon = \mu k_\perp^2 a^2$ is the eigenvalue, and

$$V(x) = -\frac{g_0}{1+x^2} + \frac{1}{(1+x^2)^2} + \sigma(1+x^2) \ , \tag{24}$$

is the effective potential.

IV. General Features

An examination of the effective potential V(x) [Eq. (24)] appearing in the mode Eq. (23) yields a wealth of information about the nature of the eigenmodes. To maintain continuity with the published literature, we again begin with the MHD limit $\sigma=0$. In Fig. 1, we have plotted V(x) as a function of x for several values of g_0. It is straightforward to see: 1) For $g_0 \leq 0$, V(x) is a monotonically decreasing function of x, resulting in an effective potential hill at x=0. Thus no localized eigenmodes around x=0 are possible for any ε. Only the continuum modes exist. 2) For $g_0 \geq 2$, V(x) has a minimum at x=0 [$V(0) = -g_0+1$], and approaches zero as x^{-2} as x goes to infinity implying a potential well at x=0. Since the potential V(x) is negative everywhere, the equation $\varepsilon-V(x) = 0$, has real solutions if and only if $\varepsilon<0$. Thus, the real turning points, and hence the bound states exist only for $\varepsilon<0$. This is the discrete spectrum of GAE. Details for this case can be seen in Ref. 8. Since there are no real turning points for $\varepsilon\geq0$, there are no bound states, and only a continuum prevails; $\varepsilon=0$ defines the lower edge of this well-known shear Alfvén continuum, 3) For $0 < g_0 < 2$, V(x) has considerably more structure with a maximum at x=0 and two minima at $x = \pm[(2/g_0)-1]^{1/2}$. Clearly for $\varepsilon\geq0$, no bound states are possible. This proves that regardless of the value of g_0, $\varepsilon\geq0$ always corresponds to the continuum modes. In this range of g_0, it is a little hard to determine the criterion which allows the existence of discrete modes for $\varepsilon<0$. The question has been dealt with in detail in Refs. 7-8, where it is shown that $g_0 > (1/4)$ is required for the discrete spectrum to be possible. The reason is, that although minimas of the potential exist, they are not deep enough to contain a mode.

The preceding discussion essentially sums up the known results, which, of course, trivially follow from a study of Eqs. (23) and (24) with $\sigma=0$.

Figure 2 contains plots of $V(x)$ versus x for several values of g_0, and for a finite but small value of $\sigma\simeq 10^{-2}$. We have chosen σ to be real for simplicity. The general nature of the following discussion will hold for a realistic complex σ.

There are several features which distinguish Fig. 2 from Fig. 1 ($\sigma=0$). The most important is the behavior of $V(x)$ as $x\to\infty$. While for $\sigma=0$, $V(x) \to 0$ as $x\to\infty$, for finite σ, $V(x) \to x^2$. For large x, the potential is like that of a simple harmonic oscillator and implies bound states for all values of g_0, because the equation $\varepsilon-V(x) = 0$ always has real solutions. Thus the erstwhile MHD continuum for $\varepsilon\geq 0$, has changed over to a discrete spectrum. Depending upon the value of g_0, the lowest eigenmode may be characterized by an eigenvalue $\varepsilon<0$. Thus, the distinction between GAE and the continuum has disappeared. They are the parts of the same discrete spectrum; the lowest eigenvalue will be positive or negative depending upon the value of g_0, which is due to the presence of equilibrium currents and ω/ω_{ci} effects.

From Fig. 2, it is also obvious that for positive g_0, the lowest mode will be localized in the potential well around $x=0$, and will not sample the form of the potential for large x. Thus its character is only mildly affected by the presence of σ. Since σ is due to the dissipative processes (for example, Landau damping for a collisionless case), the mode will have very slight damping.

The case for $g_0 \leq 0$ is altogether different. Since these modes are formed because of the turning points at large x (due to the term proportional to σ), their mode structure as well as the eigenvalue strongly depends upon σ. As a result, these modes are considerably more damped.

We remind the reader that Eqs. (23) and (24) are in the Fourier space x. The real spatial variable is $y \simeq (r-r_0)/a$. Since $p = k_\perp ax$ and y are conjugate Fourier variable, $k_\perp a\Delta x\Delta y \sim 1$, where Δx and Δy are respectively the widths in x and y. Therefore, the GAE modes, (now corresponding to the lowest modes for certain values of g_0) which are narrow in x, are relatively broad in y, possibly extending over most of the plasma. This justifies their name, Global Alfvén Eigenmodes. The exact width, however, is a function of the m number; $\Delta r \simeq r_0/|m|$, and can become quite small if $|m| \gg 1$. The discrete modes lying in the MHD continuum, however are comparatively broad in x (because of the smallness of σ), and therefore narrow in y. Thus, in real space, these modes are strongly localized around $r \simeq r_0$ (y=0). This is to be expected, because for σ=0, these modes were logarithmically singular at F=0 (y=0), and the presence of σ has simply spread the singularity in a finite region around y=0, resulting in finite amplitude everywhere.

V. Analytical and Numerical Results

The mode equation (Eq. 23) can be readily solved by numerical integration to obtain exact eigenvalues and eigenfunctions. In a later part of this section, we present our extensive numerical studies of Eq. (23).

To understand the basic features of the mode equation, we can obtain approximate analytic dispersion relations using a variety of techniques. The analytic work not only gives us important features like the scaling of the eigenvalue with various parameters, but also helps to put the numerical work in a proper perspective.

A. Variational Principle

The $\sigma=0$ limit of Eq. (23) was studied, using a variational principle, in Ref. 7, which investigates the spectrum of Global Alfvén Eigenmodes. Since Eq. (23) or equivalently Eq. (21) are self-adjoint even with $\sigma\neq 0$, an appropriate variational principle can be set up. Although Eq. (23) is more useful in delineating the general features of the system, Eq. (21) is more suitable for a variational treatment.

The functional $\left[< \quad > \equiv \int_{-\infty}^{+\infty} dx\right]$,

$$S = -\langle(1+x^2)(E_p')^2\rangle + \langle\left[\varepsilon(1+x^2) + g_0 - \sigma(1+x^2)^2\right]E_p^2\rangle \qquad (25)$$

is variational in the sense that $\delta s = 0$ reproduces the Euler equation (21). In addition, the extremal value of $S=0$.

Equation (25) can be used to obtain an eigenvalue by choosing a trial function with a variational parameter. The eigenvalue obtained is going to correspond to a radial mode number equal to the number of

nodes (zeros) of the trial function. The variational calculation can become quite involved for higher radial mode numbers. Therefore, we limit ourselves to the lowest eigenmode, and choose a trial function with no zeros for finite x,

$$E_p = e^{-\alpha x^2/2} \quad , \text{ Re } \alpha > 0 \ . \tag{26}$$

Substituting Eq. (26) into Eq. (25), and carrying out the integrals, we find

$$S \propto (\varepsilon - \sigma + g_0 - \frac{3}{4}) - \frac{\alpha}{2} + (\varepsilon - 2\sigma)\frac{1}{2\alpha} - \frac{3\sigma}{4}\frac{1}{\alpha^2} \ , \tag{27}$$

which must be solved for ε and α using the equations S=0, and

$$\frac{\partial S}{\partial \alpha} = 0 \quad = \quad -\frac{1}{2} - \frac{(\varepsilon - 2\sigma)}{2\alpha^2} + \frac{3}{2}\frac{\sigma}{\alpha^3} \ . \tag{28}$$

To proceed further, let us examine Fig. 2 once again. Clearly, for $g_0 \gtrsim 2$, there is a potential well at x=0, and the lowest mode is expected to be a GAE, essentially confined in this well with a negative eigenvalue $\varepsilon = -|\varepsilon|$. Further, the size of the well is $\Delta x \sim 1$ implying that $\alpha \simeq 1$. In this case, Eq. (28) gives ($\sigma \ll 1$)

$$\alpha = (2\sigma - \varepsilon)^{1/2} = [2\sigma + |\varepsilon|]^{1/2} . \tag{29}$$

Substituting Eq. (29) into Eq. (28), correct to order σ, we obtain

$$\varepsilon = -|\varepsilon_0| + \frac{2|\varepsilon_0| + 2|\varepsilon_0|^{1/2} + 1.5}{2|\varepsilon_0| + |\varepsilon_0|^{1/2}}\,\sigma \equiv -|\varepsilon_0| + \tau\sigma \tag{30}$$

where

$$\varepsilon_0 = g_0 - \frac{1}{4} - \left(g_0 - \frac{1}{2}\right)^{1/2} \tag{31}$$

is the already calculated result,[8] and the terms proportional to σ are the new small correction to the eigenvalue. To show that Eq. (31) implies weak Landau-damping, let us evaluate σ for the collisionless hot plasma case. The definition of hot plasma, in the present context, is that at $r=r_0$, $\omega < k_\parallel v_e$ which leads to $(\zeta)^{-1} \simeq 1-i\pi^{1/2}(\omega/k_\parallel v_e)$, and

$$\sigma = (k_\perp a)^4 \frac{k_\parallel^2 \rho_s^2}{a^2\Lambda^2}\left(1 - i\sqrt{\pi}\,\frac{v_A}{v_e}\right), \tag{32}$$

where we have used $\omega \sim k_\parallel v_A$ in the damping term. Substituting Eq. (32) into Eq. (31), and making use of the definition of ε, we obtain

$$\alpha_1 \frac{\omega^2}{v_A^2} = k_\parallel^2\left[1 + \tau k_\perp^2 \rho_s^2\left(1 - i\pi^{1/2}\,\frac{v_A}{v_e}\right)\right] - \frac{\varepsilon_0 \Lambda^2}{k_\perp^2 a^2} \tag{33}$$

Notice that σ corrections have led to a change in the real part of the frequency in addition to the damping. From Eq. (33), it is straightforward to show that

$$\frac{I_m\ \omega}{Re\ \omega} = -\frac{\tau}{2} k_\perp^2\ \rho_s^2\ \pi^{1/2}\ \frac{v_A}{v_e} \tag{34}$$

Thus Eqs. (33) and (34) are the dispersion relation for the lowest radial eig_0 enmode for the case $g_0 \gtrsim 2$. These are the mildly damped GAE.

The width of the trial function is equal to $(2/\alpha)^{1/2} = (2)^{1/2} |\varepsilon|^{-1/4}$ [Eqs. 26,29]. Thus $\Delta y = (k_\perp a)^{-1} \simeq (k_\perp a)^{-1} |\varepsilon|^{1/2} (2)^{-1/2}$ is of order unity for low m numbers. Thus the mode is radially broad, and covers a large part of the plasma.

In the range $1/4 < g_0 < 2$, the lowest eigenmode still should be a GAE, however the structure of the potential is complicated enough that Eq. (33) and (34) can only be qualitatively correct. The accuracy can be improved by using more involved trial functions, but the procedure turns out to be tedious and not very illuminating. For quantitatively correct results in this range, we depend upon our numerical solutions.

For values of $g_0 < 1/4$, there were no bound states for $\sigma=0$ (continuum modes). In this range, it is the σ dependent terms that provide the confining potential even for the lowest eigenmode. It was discussed in Sec. IV that these modes are broad in x (narrow in real space), suggesting that we seek a solution of Eq. (27) and (28) for $\alpha << 1$. Approximate solutions are

$$\alpha = \frac{3\sigma}{\varepsilon - 2\sigma}\ , \tag{35}$$

and

$$\varepsilon \simeq \left(1 - \frac{4}{3} g_0\right)^{1/2} 3\sigma^{1/2} + 2\sigma ,$$

$$\simeq \left(1 - \frac{4}{3} g_0\right)^{1/2} 3\sigma^{1/2} \qquad (36)$$

because $\sigma << 1$. Thus we already see that the eigenvalue turns out to be proportional $\sigma^{1/2}$ in contradistinction to the case $g_0 > 2$, where the changes in the eigenvalue were proportional to σ. Since σ is the measure of the damping, these modes (which were in the continuum) are much more damped as compared to the GAE. We can rewrite Eq. (36) in the form

$$\alpha_1 \frac{\omega^2}{v_A^2} = k_\parallel^2 \left[1 + \left(1 - \frac{4}{3} g_0\right)^{1/2} 3 \left|\frac{\Lambda}{k_\parallel}\right| \frac{\rho_s}{a} \left(1 - \frac{i\pi^{1/2}}{2} \frac{v_A}{v_e}\right)\right] \qquad (37)$$

from which we deduce

$$\frac{\text{Im } \omega}{\text{Re } \omega} \simeq -\left(1 - \frac{4}{3} g_0\right)^{1/2} \frac{3}{2} \left|\frac{\Lambda}{k_\parallel}\right| \frac{\rho_s}{a} \frac{\pi^{1/2}}{2} \frac{v_A}{v_e}$$

$$= -\left(1 - \frac{4}{3} g_0\right)^{1/2} \frac{3}{4} \left|\frac{\Lambda}{k_\parallel}\right| \left(\frac{\pi}{2}\right)^{1/2} \frac{c}{a\omega_{pe}} \qquad (38)$$

where c is the speed of light in vacuum, and $\omega_{pe} = (4\pi n_0 e^2/m_e)^{1/2}$ is the electron plasma frequency. Thus we notice that the damping of the erstwhile continuum modes is independent of electron temperature to leading order. It is nonzero as long as the effects of finite electron

mass are retained. It is, of course, of utmost importance to realize that the discrete spectrum is also contingent upon finite electron inertia, otherwise the system relapses to the MHD shear Alfvén continuum. Equation (38) clearly shows why the damping of the continuum modes is essentially independent of the model for describing electron parallel dynamics. The radial width of this mode can be computed using Eqs. (32) and (35), and is

$$\Delta y = \frac{r-r_0}{a} = \left(\frac{k_\parallel^2 \rho_s^2}{\Lambda^2 a^2}\right)^{1/4} \simeq \left(\frac{\rho_s}{a}\right)^{1/2} \ll 1 \ . \tag{39}$$

B. Higher Radial Eigenmodes

Although for most practical applications (for example, the Alfvén wave heating or current drive), the lowest radial eigenmode of Alfvén waves (whether a GAE, or the continuum kind) is important, it is of some interest to calculate the higher radial eigenmodes. The reader is referred to Ref. 7 for a calculation for the GAE's (σ=0). We concentrate here on the case when $g_0 \lesssim 1$, and solve Eq. (23) for higher radial mode numbers. Since the turning points of the equation are determined by the term proportional to σ, we choose to solve the simplified simple harmonic oscillator equation

$$\psi'' + [\varepsilon - \sigma - \sigma x^2]\psi = 0 \ , \tag{40}$$

which has a spectrum

$$\varepsilon_n = \sigma + (2n+1)\sigma^{1/2} \simeq (2n+1)\sigma^{1/2} \tag{41}$$

where n is the radial quantum number. The solution (40) is approximately correct if and only if the neglected terms are small compared to the terms that are kept. We estimate the value of the neglected terms at the turning points [which are the solution of $(1+x_t^2) = \varepsilon_n/\sigma = (2n+1)/\sigma^{1/2}$ to be $g_0(1+x_t^2)^{-1} + (1+x^2)^{-2} \simeq g_0\sigma^{1/2}/(2n+1)$. Thus the ratio of the neglected terms to the retained terms is $g_0/(2n+1)^2$ and becomes much smaller than unity for very large n numbers. Thus, the dispersion relation Eq. (40) is correct strictly in the large n limit. The eigenvalue turns out to be independent of g_0 because for very high n, the structure of the potential near x=0 is quite unimportant. Another interesting feature is that the eigenvalue scales as $\sigma^{1/2}$, which makes high n modes relatively strongly damped. In addition, the damping increases with increasing n.

The main analytic results of this paper are: 1) Eqs. (33) and (34) describing the mildly damped lowest radial eigenmode of the GAE variety, with its characteristic frequency below the boundary of the MHD shear Alfvén continuum (F=0). The damping is clearly a function of the model for parallel electron dynamics, 2) Eqs. (37) and (38), which describe the comparatively strongly damped lowest eigenmode of the discrete spectrum of what was the Alfvén continuum ($F \geq 0$). The damping of the mode seems to be quite insensitive to the model for parallel electron dynamics, 3) Eq. (41), which is the dispersion relation for very high ($n \gg 1$) radial mode numbers, and is independent of g_0. The damping rate increases with increasing n, and is essentially independent of the model of electron dynamics.

C. Numerical Solution

In Sections VA and VB, we derived several approximate analytic dispersion relations which are valid in different parameter regimes. In this section, we present numerical solutions of Eq. (23) for the eigenvalues as well as the eigenfunctions. We also compare the numerical results with the analytical formulas.

In our numerical work, we have used

$$\Sigma_n = -\varepsilon_n \tag{41}$$

to be the eigenvalue. Thus $\mathrm{Im}\Sigma_n > 0$ implies damping. Further $\mathrm{Re}\Sigma_n > 0$ corresponds now to the GAE, while $\mathrm{Re}\Sigma_n < 0$ corresponds to the modes of the erstwhile continuum. Notice that all modes, discussed in this paper, are damped.

In Figs. 3-6, we show plots of the real and imaginary parts of Σ_n versus g for two different choices of σ: the weakly dissipative case with $\sigma = (1-i/2) \times 10^{-4}$ (Figs. 3-4), and the relatively strongly dissipative case with $\sigma = (1-i/2) \times 10^{-2}$ [Figs. 5-6]. Several features of the eigenvalues, qualitatively discussed in Sec. IV, can be easily seen. First and foremost is that the distinction between GAE and the continuum modes has disappeared. As the radial quantum number n is varied, the real part of Σ changes from positive ($\varepsilon<0$, GAE) to negative ($\varepsilon>0$, continuum). There is no accumulation point at $\Sigma = 0 = \varepsilon$. This happens for all values of g_0. For the weakly dissipative case (Figs. 3-4), the real part of the eigenvalue Σ_n is positive only for n=0 and n=1. Of course, if the value of g is increased, a larger and

larger number of modes would have $Re\Sigma_n > 0$. Very large values of g, however, are quite unphysical. It is of interest to note that the damping rate for the n=0 mode suddenly drops at $g_0 \simeq 0.6$, which is also the threshold for the existence of a GAE (the value of g_0 at which $\Sigma_0 = 0$). Thus, we find that the damping rate decreases rather rapidly as the mode changes its character from a continuum mode to a Global Alfvén Mode. For the stronger damping case, [Figs. (5-6)], the transition occurs at $g_0 \simeq 1$. We would like to remark that the eigenvalue for the fundamental mode is very accurately given by Eq. (31) for $g_0 \gtrsim 2$. Significant departure from Eq. (31) occurs for those values of g_0 for which $\Sigma_0 \simeq 0$. Similarly, the formula given by Eq. (36) quite accurately describes the eigenvalues for $g_0 < 0$.

In Figs. 7-8, we plot the real and imaginary parts of the eigenvalue versus σ for $g_0 = 0$. We have picked this case because for $g_0 = 0$, there are no GAE's and hence, there is no discrete spectrum without σ. This is amply confirmed by our numerical experiments because the code does not converge as σ approaches zero. Once σ is turned on, we can find a whole series of the modes of discrete spectrum. In Figs. 7-8, we have also plotted Eq. (36). It is clear that the agreement between the analytical formula and the numerical results is very good. Although Eq. (40) was derived to be true only for $n \gg 1$, it is in fair agreement with the numerical curve for n=5. The scaling $\Sigma \propto \sigma^{1/2}$ is true for all the radial modes.

We now show the plots of the eigenfunctions corresponding to the first three radial eigenmodes [n=0,1,2] for $\sigma = (1-i/2) \times 10^{-4}$, and for two distinct values of g_0. Figures 9-11 correspond to the case $g_0 = 2$, (for which the lowest two eigenmodes have $Re\Sigma > 0$), while Figs. 12-14

correspond to the case $g_0 = 0$. Notice that the eigenfunction for the n=0, $g_0 = 2$ case, which corresponds to the GAE, is much narrower in x than the eigenfunctions corresponding to the other displayed modes. Hence in real space, which is the space, conjugate to x, the GAE does indeed turn out to be much broader than the continuum modes.

Discussion and Conclusions

We have derived, using a kinetic theory, a fourth order differential equation which describes the properties of Alfvén waves in an inhomogeneous, current carrying, dissipative cylindrical plasma. By solving this equation analytically and numerically, we have shown that the Alfvén waves are described by a discrete spectrum. This discrete spectrum replaces the well-known MHD continuum, and also encompasses the discrete spectrum of Global Alfvén Waves (made possible by the effects of plasma current and finite ω/ω_{ci} together with cylindrical curvature) which now ceases to have an accumulation point at $\varepsilon=0$.

We have also derived analytical formulas which approximate the dispersion relation in various limiting cases. The analysis is augmented as well as verified by numerical solutions of the eigenmode equation. We have shown that, depending upon the value of the parameter g_0 [see Eq. (8), and the discussion following Eq. (18)], the fundamental radial mode (n=0) is either a Global Alfvén Eigenmode localized in the potential well near x=0 [see Fig. (2)], or a mode of the old MHD continuum which is now localized in the potential well created by the dissipative terms. The former is relatively unaffected by the dissipation, and is mildly damped [Eqs. (31)-(34)]. The latter, on the other hand, becomes a discrete mode only due to dissipation, and is thus relatively strongly damped [Eqs. (36)-(38)]. In the real space [which is conjugate to x], the GAE type of modes are rather broad, while the continuum type of modes are rather narrow.

The higher radial eigenmodes are more strongly damped; the damping rate is directly proportional to n. The dispersion relation for these

high n modes is essentially independent of g_0. Because of their larger damping, these modes are not of great interest.

The fundamental (n=0) mode of the Alfvén waves is the least damped mode, and is being extensively investigated for its possible use in heating thermonuclear plasmas. The current analysis, delineates several crucial properties of this mode. Thus our analysis, in addition to its being of intrinsic scientific interest, can also be useful in determining optimum conditions for Alfvén wave heating.

Acknowledgments

The author expresses his gratitude to Dr. Joe Sedlak for providing the numerical solutions of the mode equation. Discussion with Dr. David W. Ross and Mr. Y. M. Li are also acknowledged.

References

1. W. Grossman and J. Tataronis, Z. Phys. 261, 217(1973).

2. J. P. Goedbloed, Phys. Fluids 18, 1258(1975), and references therein.

3. M. N. Rosenbluth and P. H. Rutherford, Phys. Rev. Lett. 34, 1428(1975).

4. J. W. Connor, W. M. Tang, and J. B. Taylor, Phys. Fluids 26, 158(1983).

5. J. F. Drake and R. Kleva, Phys. Fluids 24, 1499(1981).

6. D. W. Ross, G. L. Chen, and S. M. Mahajan, Phys. Fluids 25, 652(1982).

7. K. Appert, R. Gruber, F. Troyon, and J. Vaclavik, Lausanne Report LRP 200/81, December 1981.

8. S. M. Mahajan, D. W. Ross and G. L. Chen, Phys. Fluids 26, 2195(1983).

9. A. Hasegawa and L. Chen, Phys. Rev. Lett. 32, 454(1974).

10. Y. P. Pao, Nucl. Fusion 14, 25(1974).

Figure Captions

1. $V(x)$ versus x for the MHD limit $\sigma=0$. The curves have different values of $g_0 \equiv g$. Notice that $V(x) \to 0$ as $x \to \infty$ for all the curves.
2. $V(x)$ versus x for the dissipative case, $\sigma = 10^{-2}$. The potential well at large x is responsible for the discrete spectrum.
3. The real part of the eigenvalue $\Sigma_n = -\varepsilon_n$ for several radial eigenmodes as a function of g for weak dissipation $\sigma = (1-i/2) \times 10^{-4}$.
4. Imaginary Σ_n for the same parameters as Fig. 3.
5. Real Σ_n versus g for $n=0$ to 5, and relatively strong dissipation $\sigma = (1-i/2) \times 10^{-2}$.
6. Imaginary Σ_n versus g for the same parameters as Fig. 5.
7. Real Σ_n versus σ for $g=0$ and $n=0$ to 5. The crosses (xx) represent the analytical results given by Eq. (36).
8. Imaginary Σ_n versus σ for $g=0$, and $n=0$ to 5. The crosses (xx) represent the analytical results given by Eq. (36).
9. The wave functions ψ versus x for the lowest radial mode $n=0$, and $g=2$.
10. The wave function $\psi \equiv \psi_R + i\Psi_I$ versus x for $g=2$, $n=1$.
11. The wave function ψ versus x for $g=2$, $n=2$.
12. The wave function ψ versus x for $g=0$, $n=0$.
13. The wave function ψ versus x for $g=0$, $n=1$.
14. The wave function ψ versus x for $g=0$, $n=2$.

Appendix A

Fourth Order Equation

We calculate E_r from Eq. (1), and substitute it into Eq. (2) to obtain

$$\left(F + \frac{d}{dr}\frac{1}{r}\frac{d}{dr}\,r\right)E_\perp = -\left[k_\parallel k_\perp + \frac{(r\delta')'}{r} - \frac{\delta}{r^2} + 2\delta'\frac{d}{dr}\right]E_\parallel$$

$$+ \left(S + A + \frac{d}{dr}\,k_\perp\right)\frac{1}{D}\left(S + A - \frac{k_\perp}{r}\frac{d}{dr}\right)rE_\perp \qquad \text{(A-1)}$$

$$- \left(S + A + \frac{d}{dr}\,k_\perp\right)\left[\frac{k_\parallel}{D}E'_\parallel + \frac{(r\delta)'}{r}\frac{k_\perp}{D}E_\parallel\right]$$

where $D = F - k_\perp^2$. Since $E_\parallel$ is a small quantity, and S and A are much smaller than $k_\perp$, we neglect (S+A) with respect to $\frac{d}{dr}\,k_\perp$ in the last term of the right-hand side of Eq. (A-1). The result is

$$\left(F + \frac{d}{dr}\frac{F}{rD}\frac{d}{dr}\,r\right)E_\perp - \left\{\left[\frac{k_\perp(S+A)}{rD}\right]'r + \frac{(S+A)^2}{D}\right\}E_\perp \qquad \text{(A-2)}$$

$$= -\left[k_\parallel k_\perp + \frac{(r\delta')'}{r} + \frac{\delta}{r^2} - 2\delta'\frac{d}{dr}\right]E_\parallel - \frac{d}{dr}\left[\frac{k_\parallel k_\perp}{D}\frac{d}{dr} + \frac{(r\delta)'}{r}\frac{k^2_\perp}{D}\right]E_\parallel$$

For shear Alfvén waves $\frac{\alpha_1\omega^2}{v_A^2} \simeq k_\parallel^2$, and for most problems of interest $k_\perp^2 >> k_\parallel^2$. Thus approximating $D \simeq -k_\perp^2 \simeq -(m/r)^2$, we can considerably simplify Eq. (A-2). After some straightforward algebra, we can show that,

$$\frac{d}{dr}\left[\frac{(r\delta)'}{r}\right]E_\parallel - \frac{(r\delta')'}{r}E_\parallel + \frac{\delta}{r^2}E_\parallel = \left(\frac{\delta}{r} + \delta'\right)E'_\parallel\,, \qquad \text{(A-3)}$$

which, coupled with the fact that [see Eq. 5]

$$\frac{d}{dr}\left(\frac{k_\parallel}{k_\perp}\right) \simeq \frac{1}{m}\frac{d}{dr}\left(rk_\parallel\right) = \frac{k_\parallel}{m} + \left(\delta' - \frac{\delta}{r}\right) , \tag{A-4}$$

changes Eq. (A-2) to the form

$$\left(F - \frac{d}{dr}\frac{F}{rk_\perp^2}\frac{d}{dr}\,r\right)E_\perp + gE_\perp$$

$$= \frac{k_\parallel}{rk_\perp}\left(\frac{d}{dr}\,r\,\frac{dE_\parallel}{dr} - rk_\perp^2 E_\parallel\right) \tag{A-5}$$

where

$$g = \frac{(S+A)'}{k_\perp} + \frac{(S+A)^2}{k_\perp^2} . \tag{A-6}$$

Appendix B

Expansion around r_0

Let $k_\parallel^2 v_\parallel^2$ have a minimum at $r=r_0$, i.e.

$$\left(k_\parallel^2 v_A^2\right)'_{r=r_0} = 0 \qquad \text{(B-1)}$$

Since $v_A = B/(4\pi n_i m_i)^{1/2}$, Eq. (B-1) implies

$$2\left(\frac{k_\parallel'}{k_\parallel}\right)_{r_0} = \left(\frac{1}{n_i}\frac{dn_i}{dr}\right)_{r_0} = -\frac{1}{L_n}. \qquad \text{(B-2)}$$

Expanding F around $r=r_0$, and using (B-2),

$$F = F_0 + (r-r_0)(F')_{r_0} + \frac{1}{2}(r-r_0)^2(F'')_{r_0}\ ; \qquad \text{(B-3)}$$

where

$$F_0 = \left(\alpha_1 \frac{\omega^2}{v_A^2} - k_\parallel^2\right)_{r_0} \equiv \alpha_1 \frac{\omega^2}{v_A^2} - k_\parallel^2\ ,$$

$$(F')_{r_0} = -\frac{F_0}{L_n}\ , \qquad \text{(B-4)}$$

$$(F'')_{r_0} = -2\frac{\Lambda^2}{a^2}\ ,$$

with

$$\Lambda^2 = \frac{\alpha_1 \omega^2}{v_0^2} + a^2 (k_\parallel^2)_{r_0} \quad . \tag{B-5}$$

In deriving Eq. (B-5), we have assumed a parabolic density profile, $n_i = n_0(1-r^2/a^2)$, where a is the minor radius of the tokamak. This assumption is not at all essential. Also v_0 is the Alfvén speed at the center of the discharge. The important point to notice is that

$$\Lambda^2 \simeq \frac{\alpha_1 \omega^2}{v_A^2} + k_\parallel^2 >> F_0 = \alpha_1 \frac{\omega^2}{v_A^2} - k_\parallel^2 \simeq 0 \ , \tag{B-6}$$

because, we are interested in modes near F≃0. Within the context of Eqs. (B-1)-(B-6), we can easily show that

$$F = -\Lambda^2 (y^2 - \mu) \tag{B-7}$$

where

$$y \simeq \frac{r-r_0}{a} + \frac{F_0}{2\Lambda^2} \frac{a}{L_n} \ ,$$

and (B-8)

$$\mu = \frac{F_0}{\Lambda^2} \left[1 + \frac{1}{4} \frac{F_0}{\Lambda^2} \frac{a^2}{{L_n}^2} \right] \ ,$$

where all the quantities are evaluated at $r=r_0$.

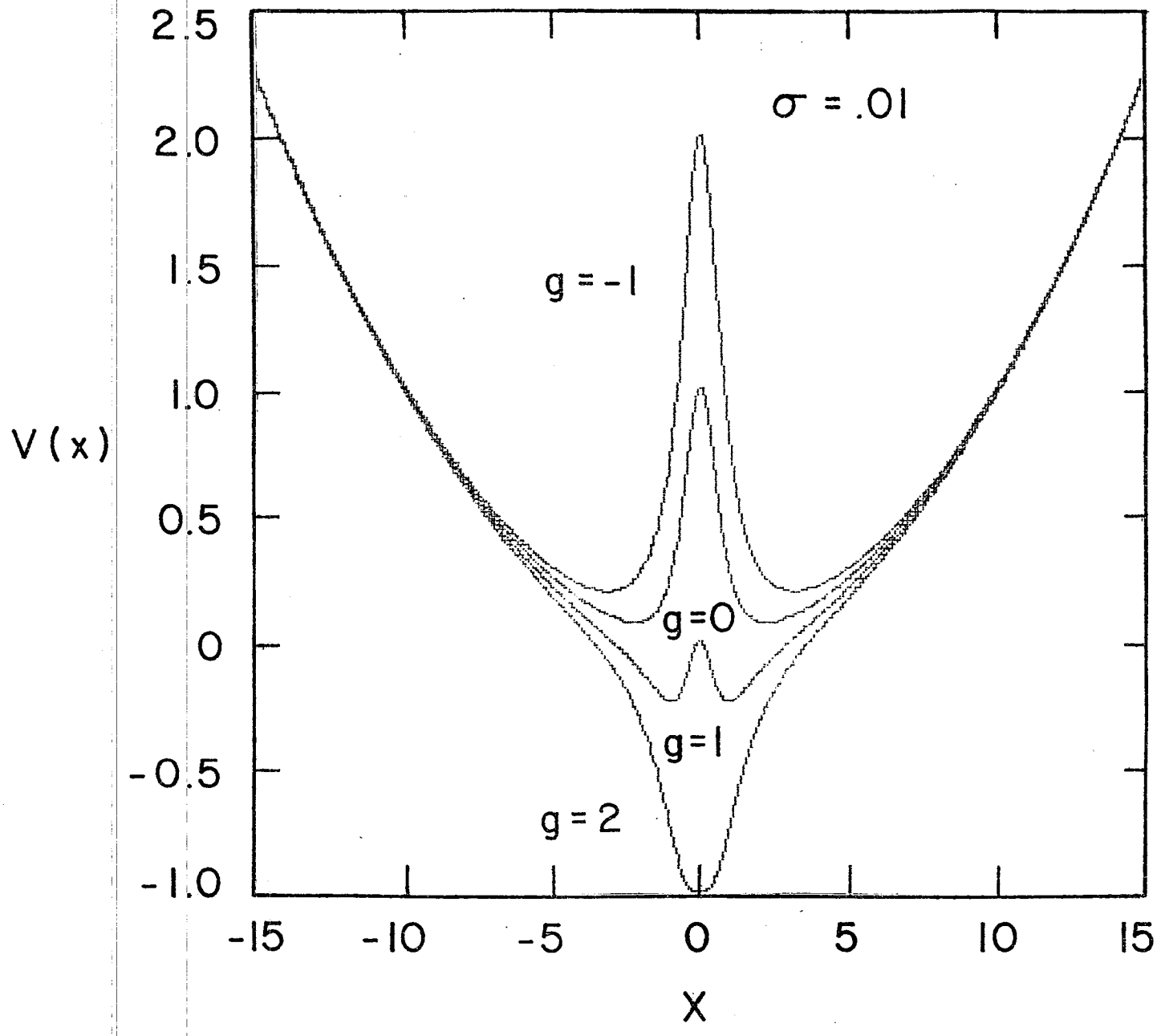

FIG. 2

by S. Rodriguez
for Joe Sedlak

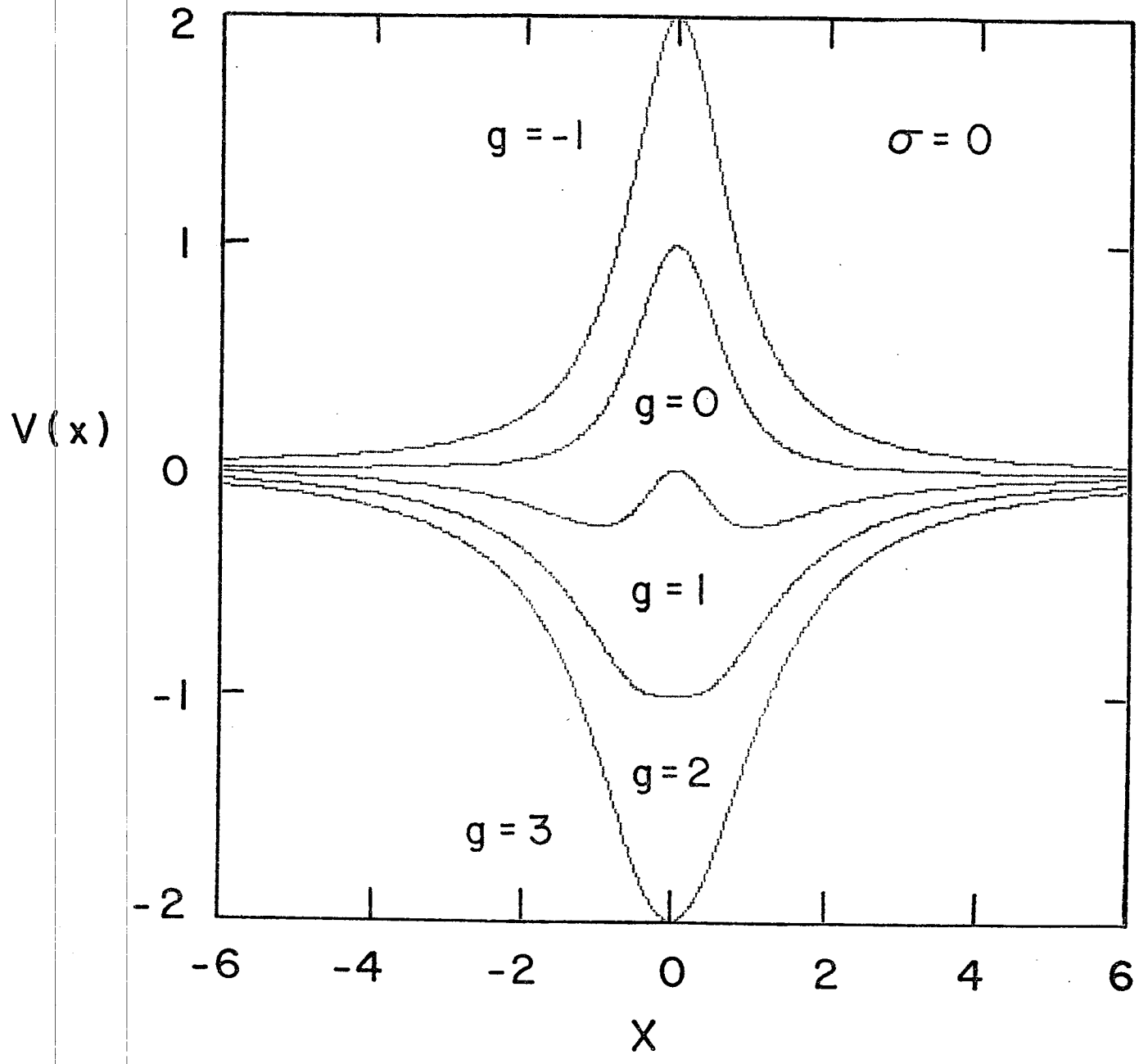

FIG. 1

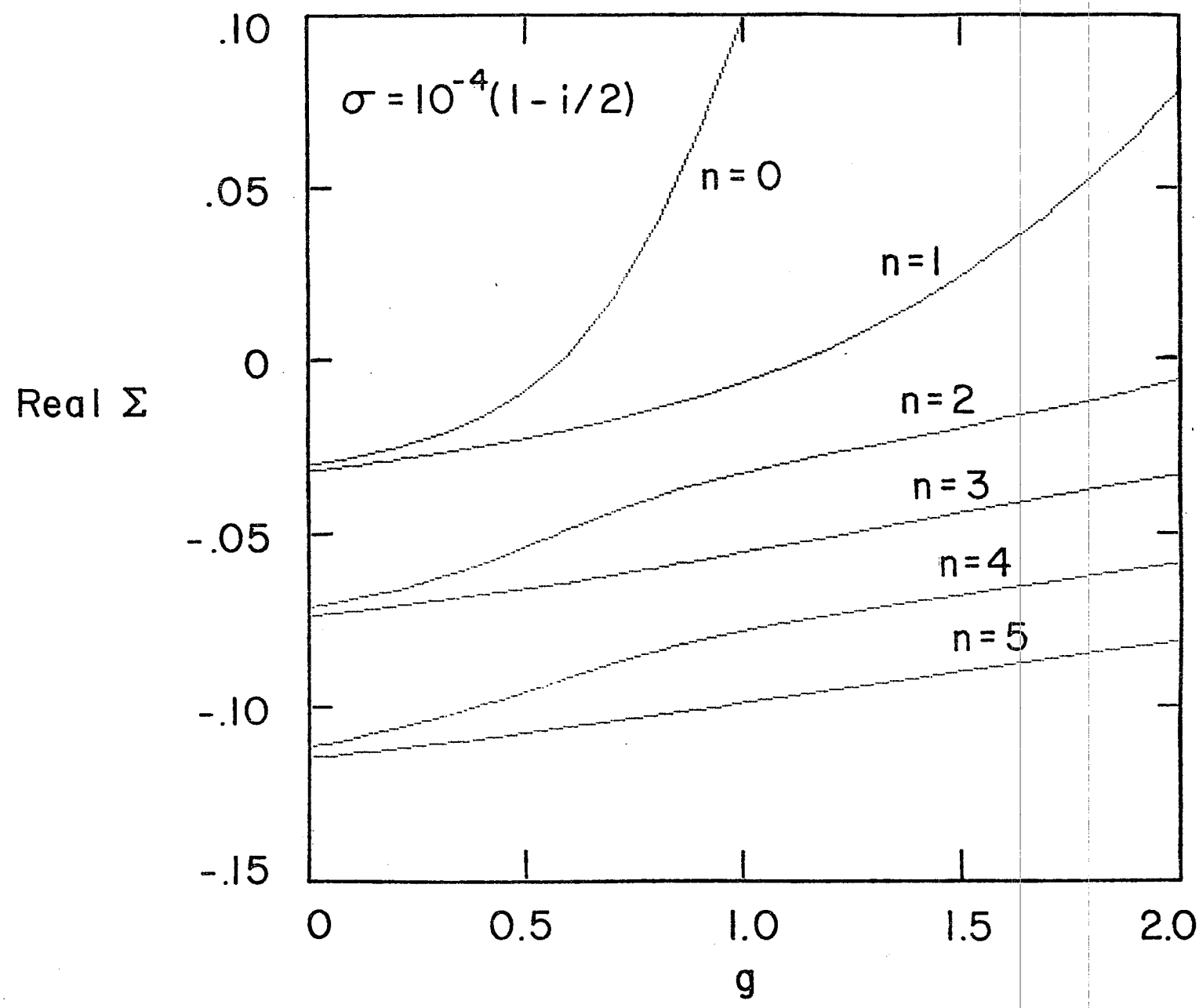

FIG. 3

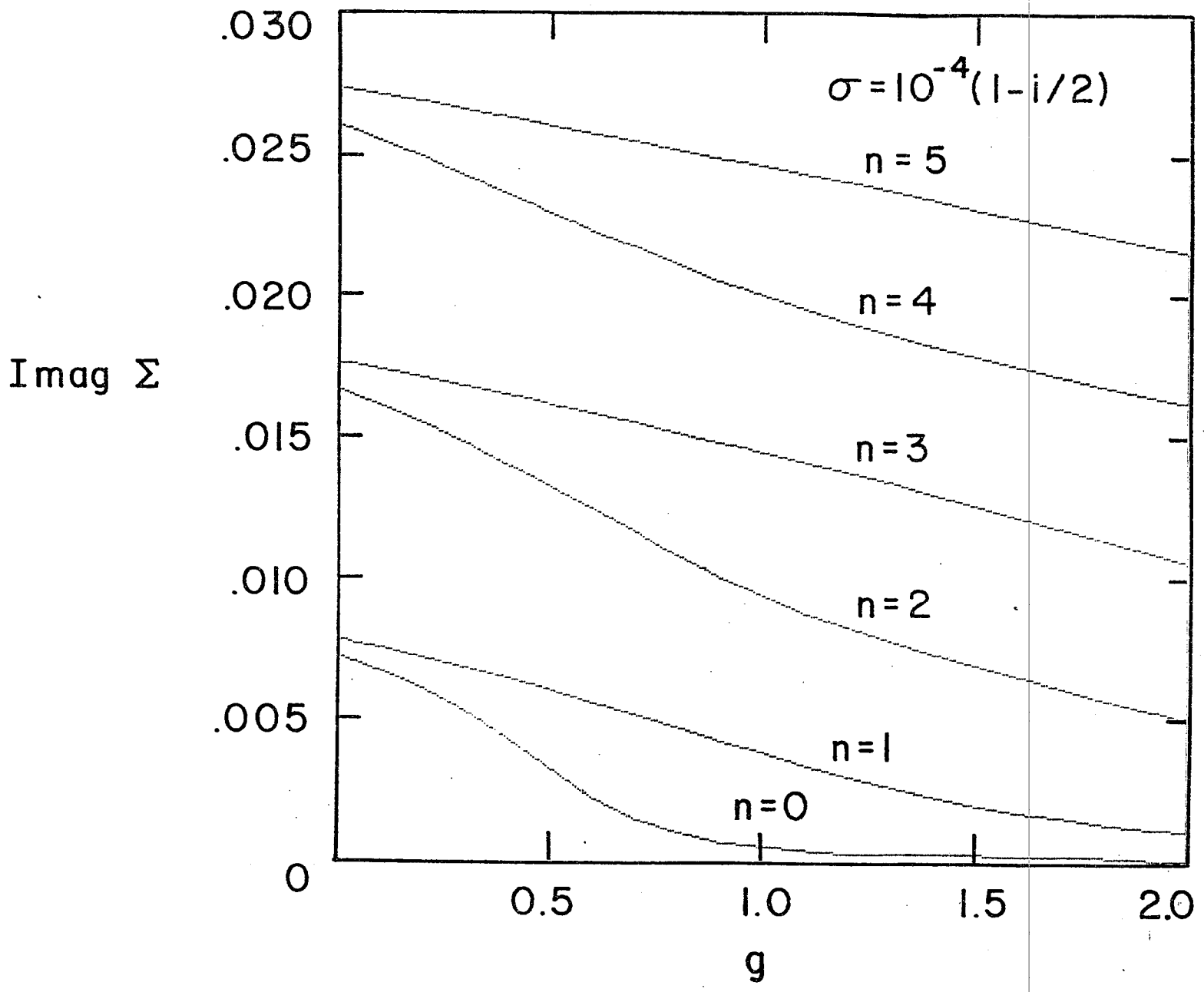
.030
.025
.020
.015
.010
.005
0
Imag Σ
σ = 10^-4 (1 - i/2)
n = 5
n = 4
n = 3
n = 2
n = 1
n = 0
0.5
1.0
1.5
2.0
g

FIG. 4

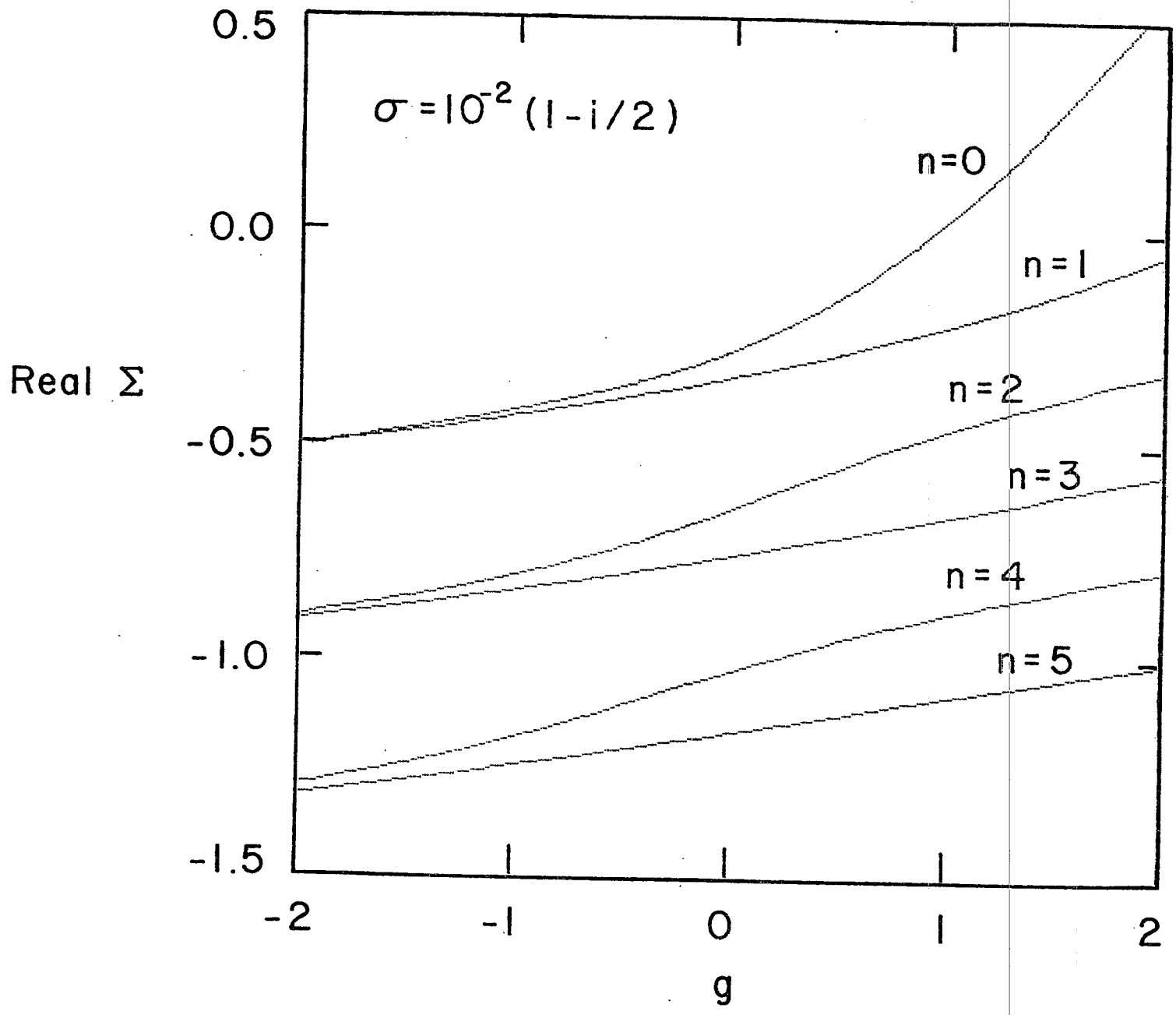

FIG. 5

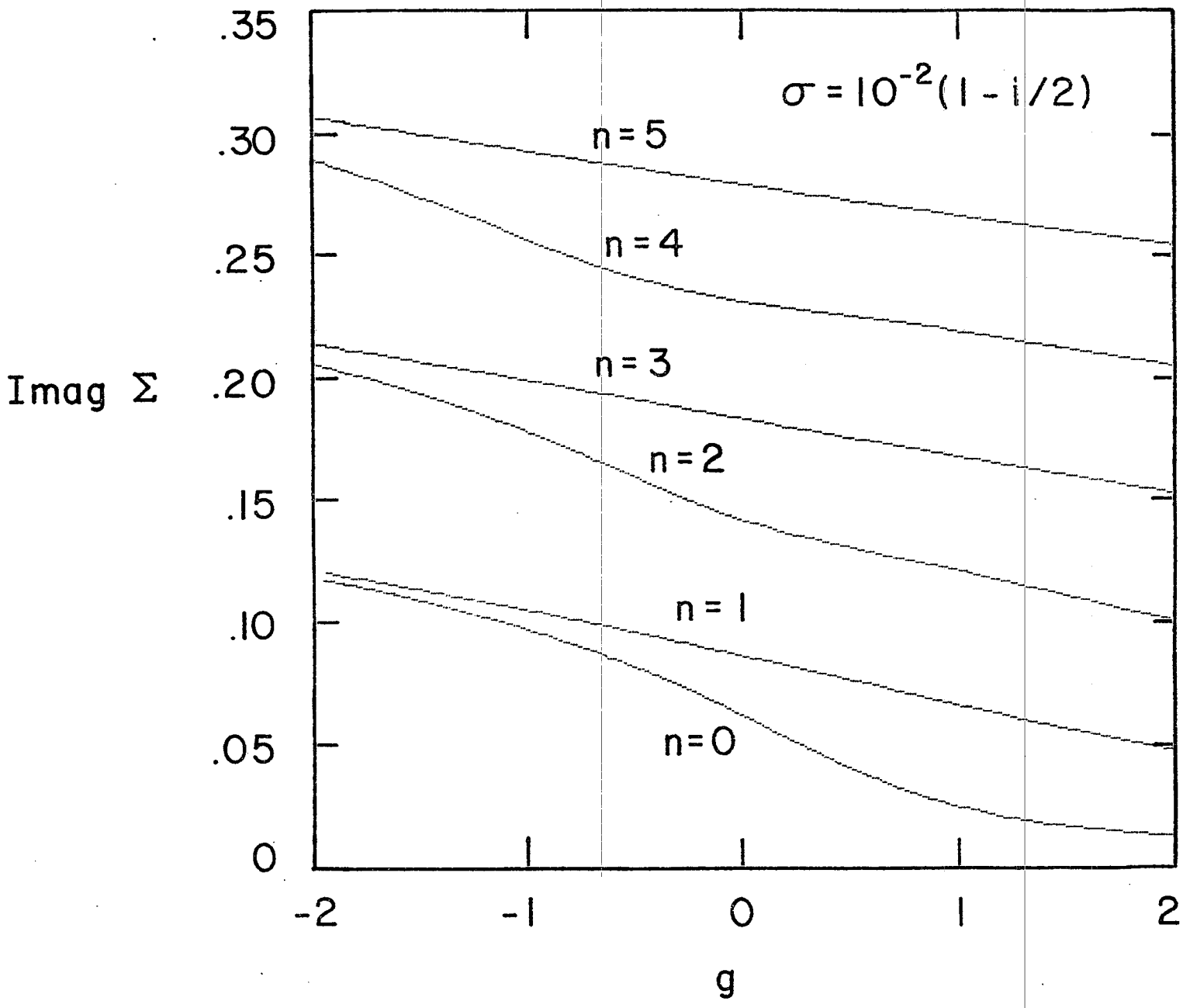

FIG. 6

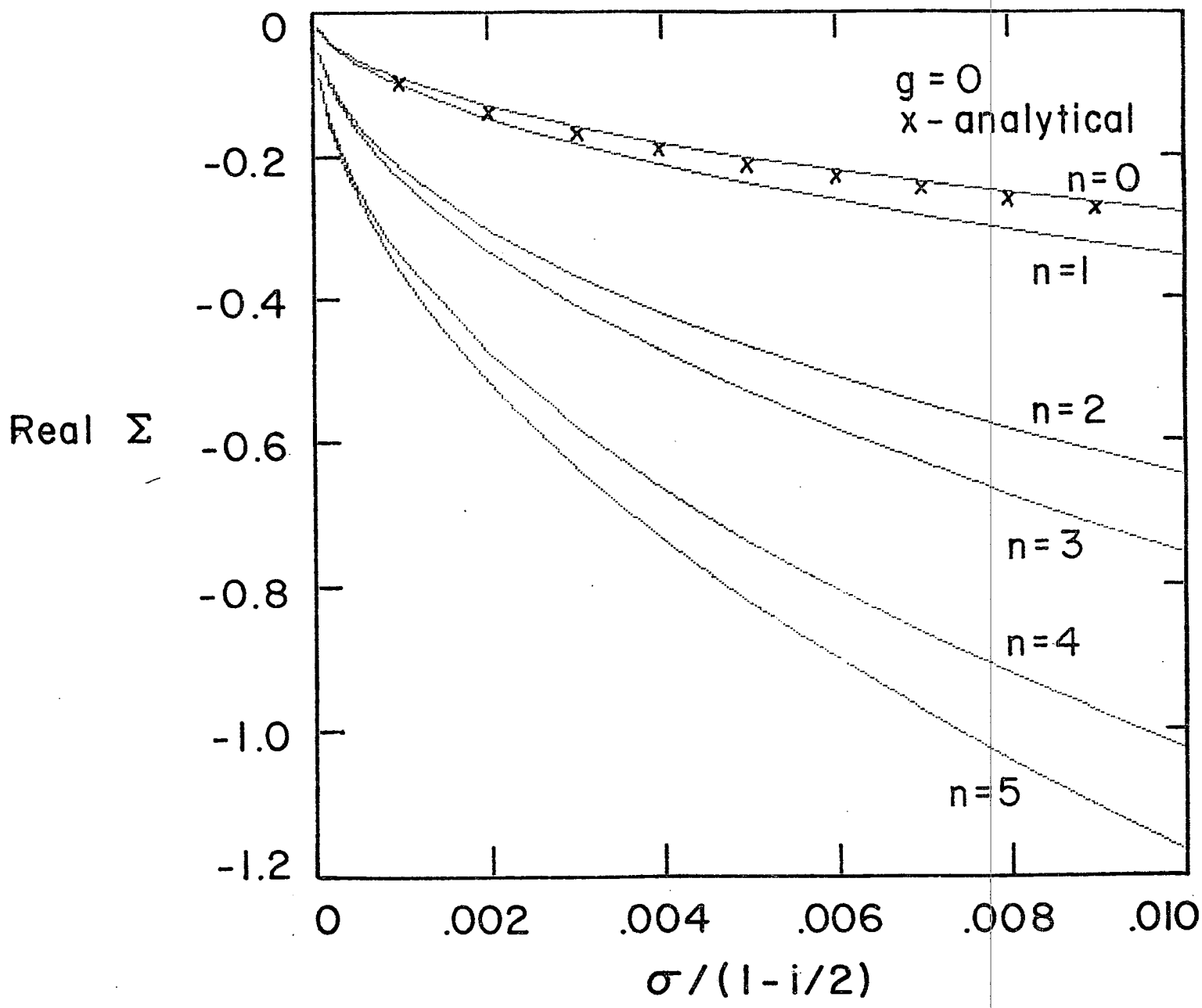
Real Σ
0
-0.2
-0.4
-0.6
-0.8
-1.0
-1.2
0
.002
.004
.006
.008
.010
σ/(1-i/2)
g = 0
x - analytical
n=0
n=1
n=2
n=3
n=4
n=5

FIG. 7

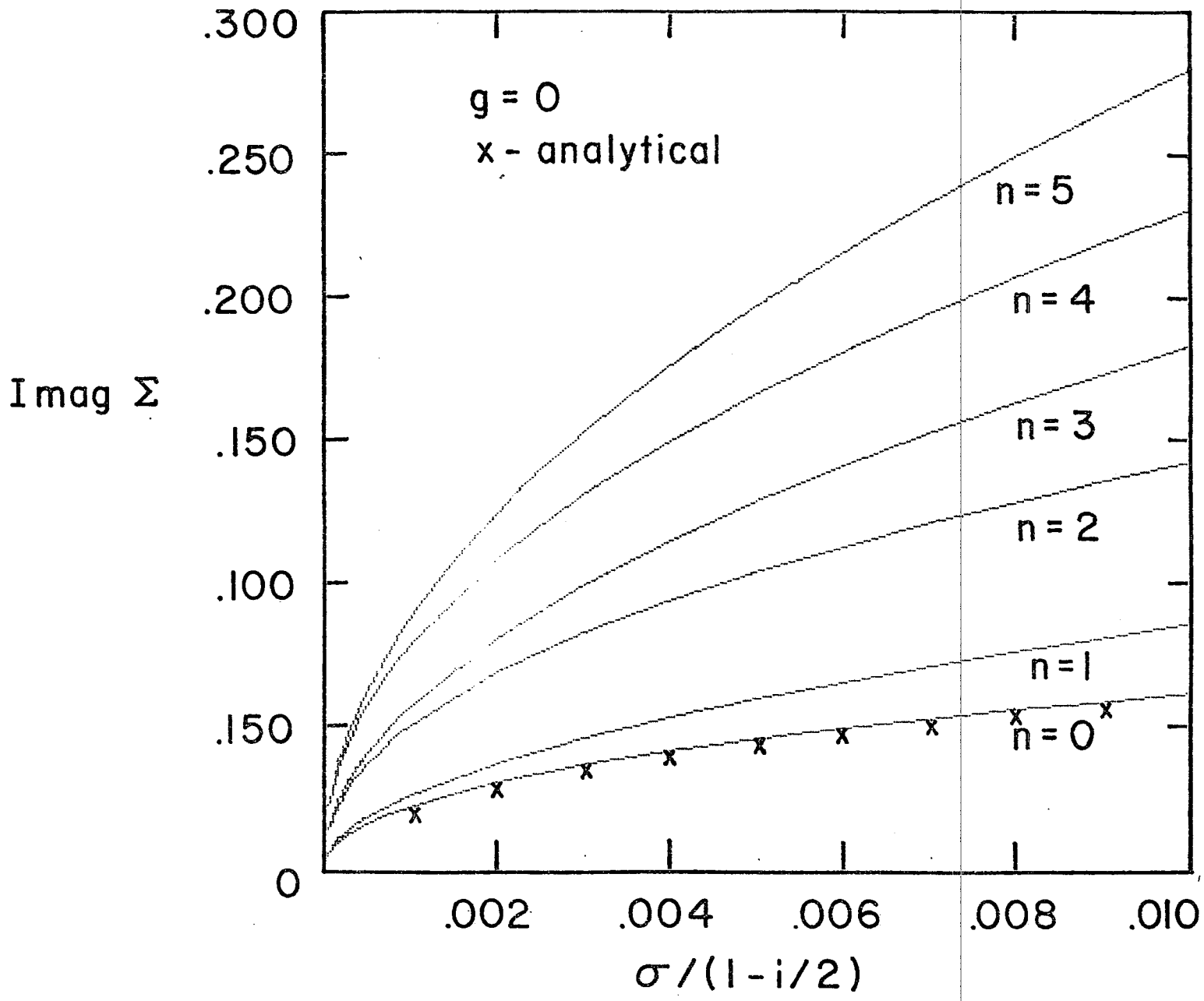
.300
.250
.200
.150
.100
.150
0
Imag Σ
g = 0
x - analytical
n = 5
n = 4
n = 3
n = 2
n = 1
n = 0
.002
.004
.006
.008
.010
σ/(1-i/2)

FIG. 8

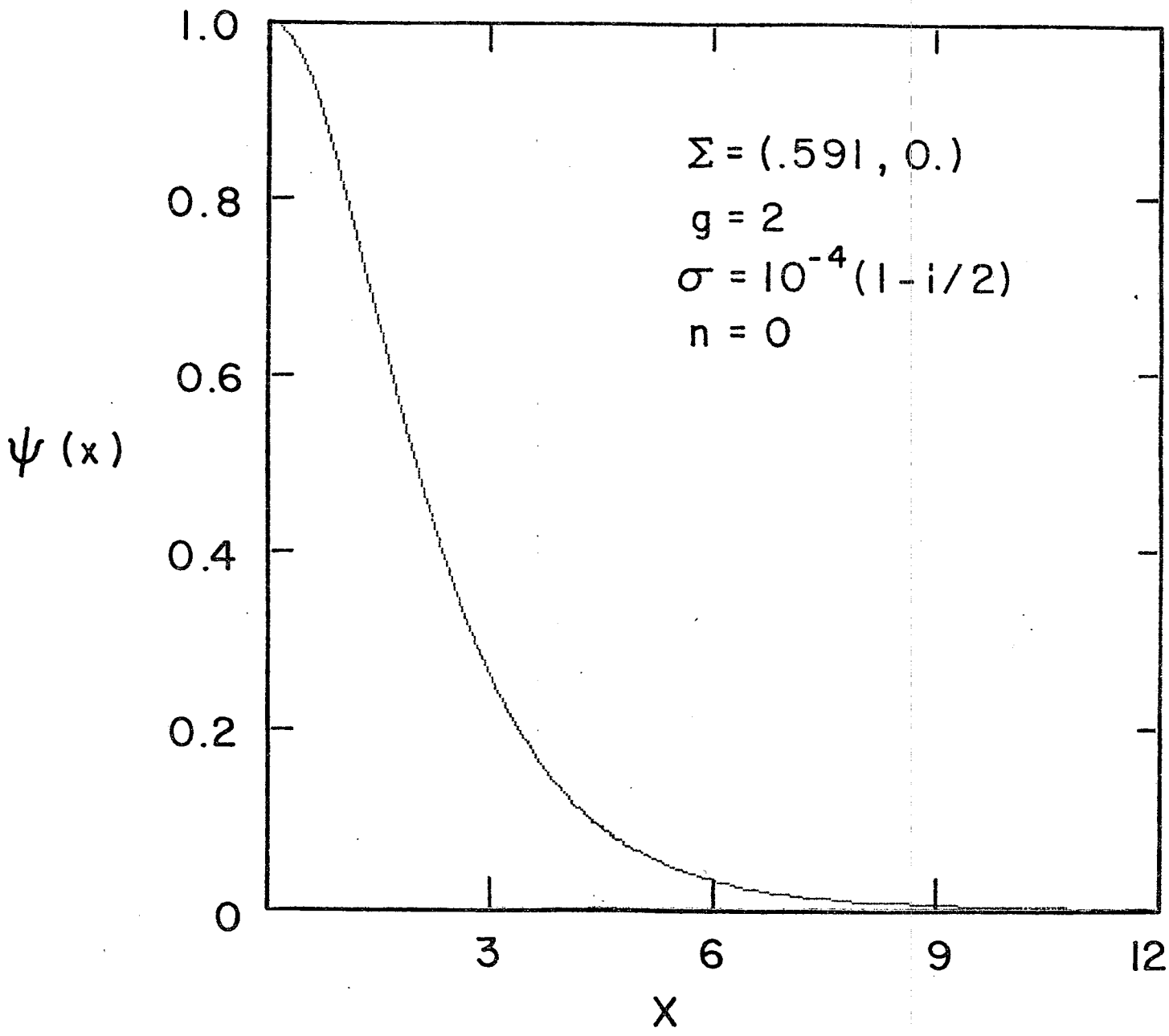

FIG. 9

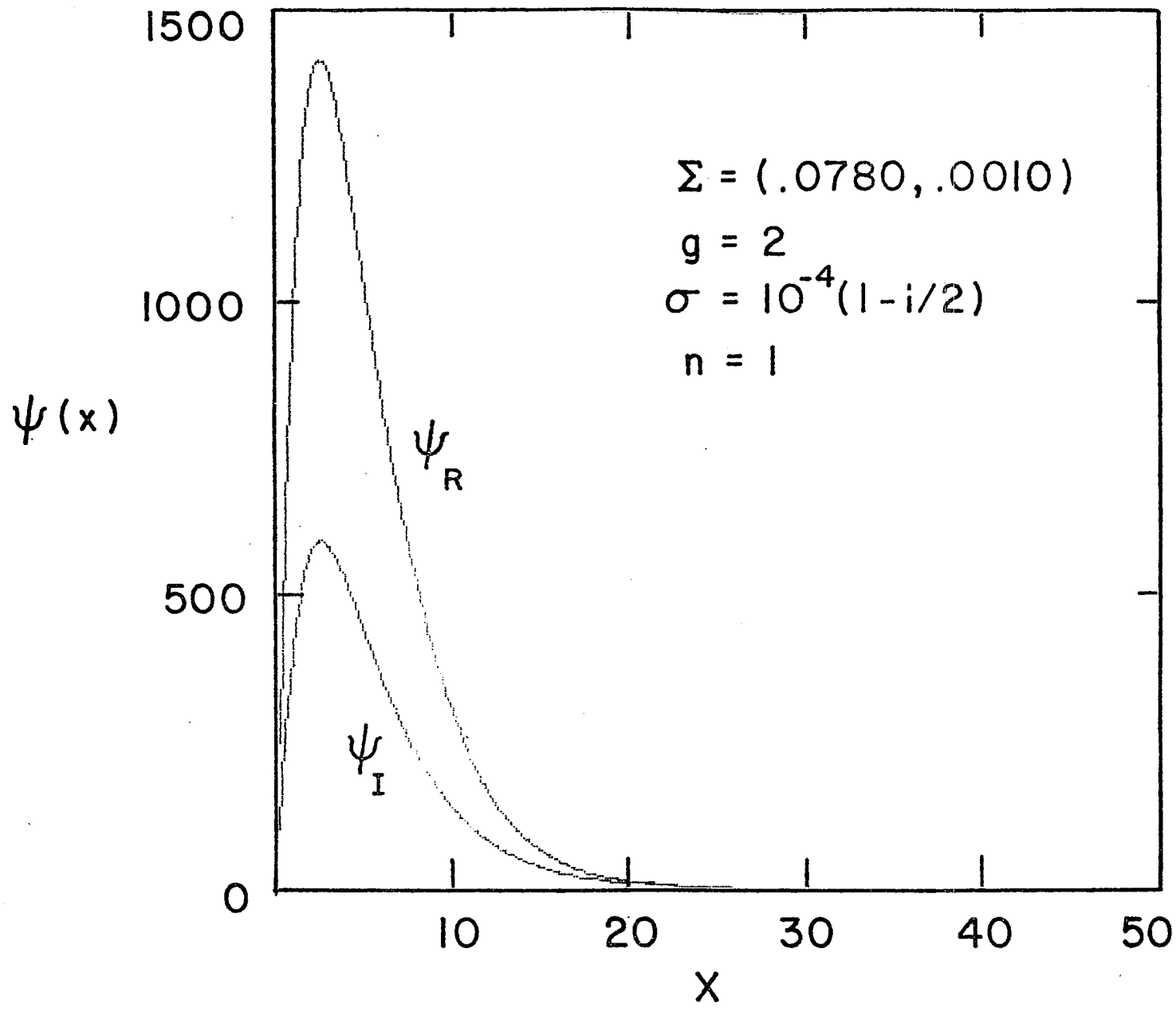

FIG. 10

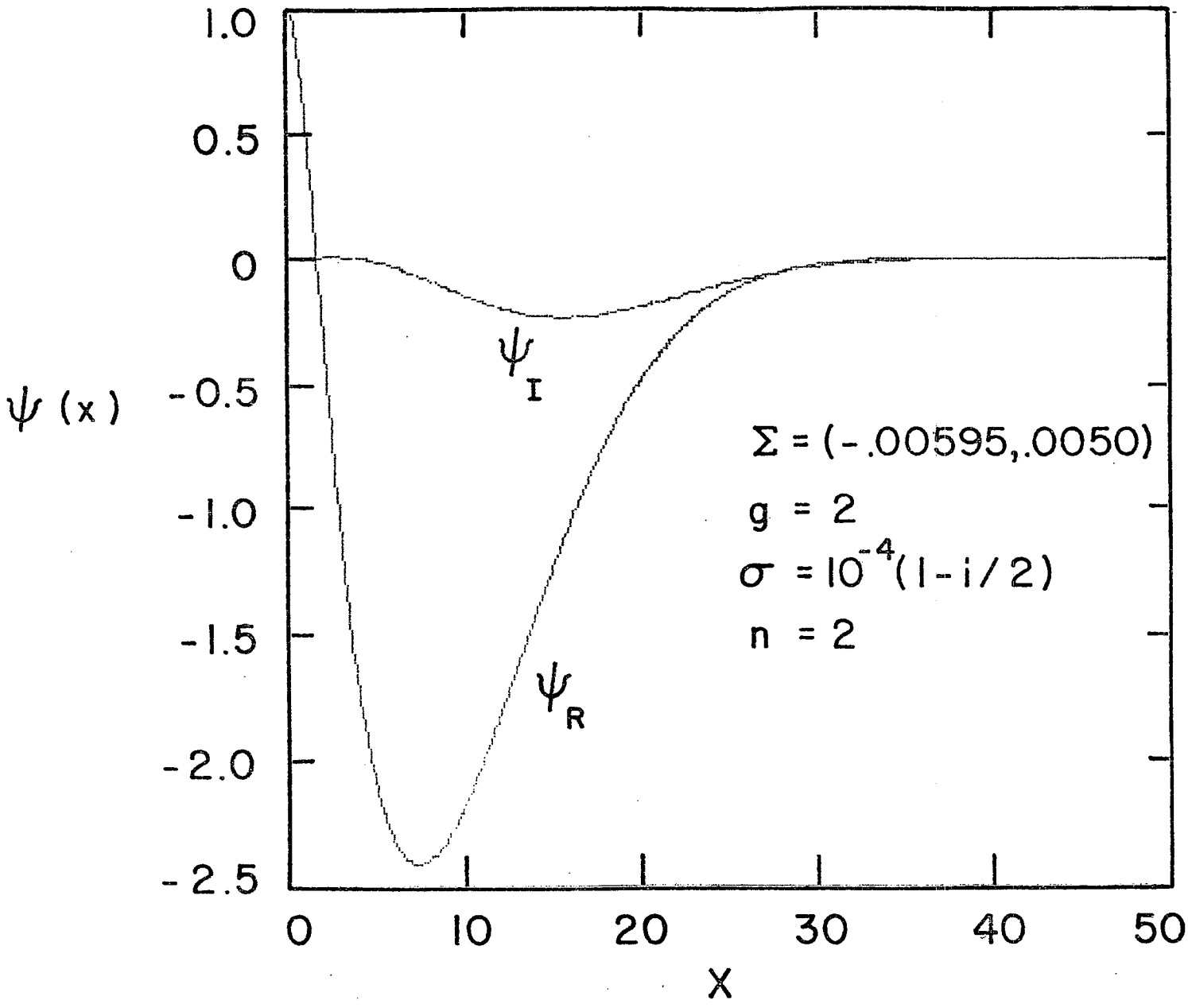
1.0
0.5
0
-0.5
-1.0
-1.5
-2.0
-2.5
ψ (x)
ψ_I
ψ_R
Σ = (-.00595,.0050)
g = 2
σ = 10^-4(1-i/2)
n = 2
0
10
20
30
40
50
X

FIG. 11

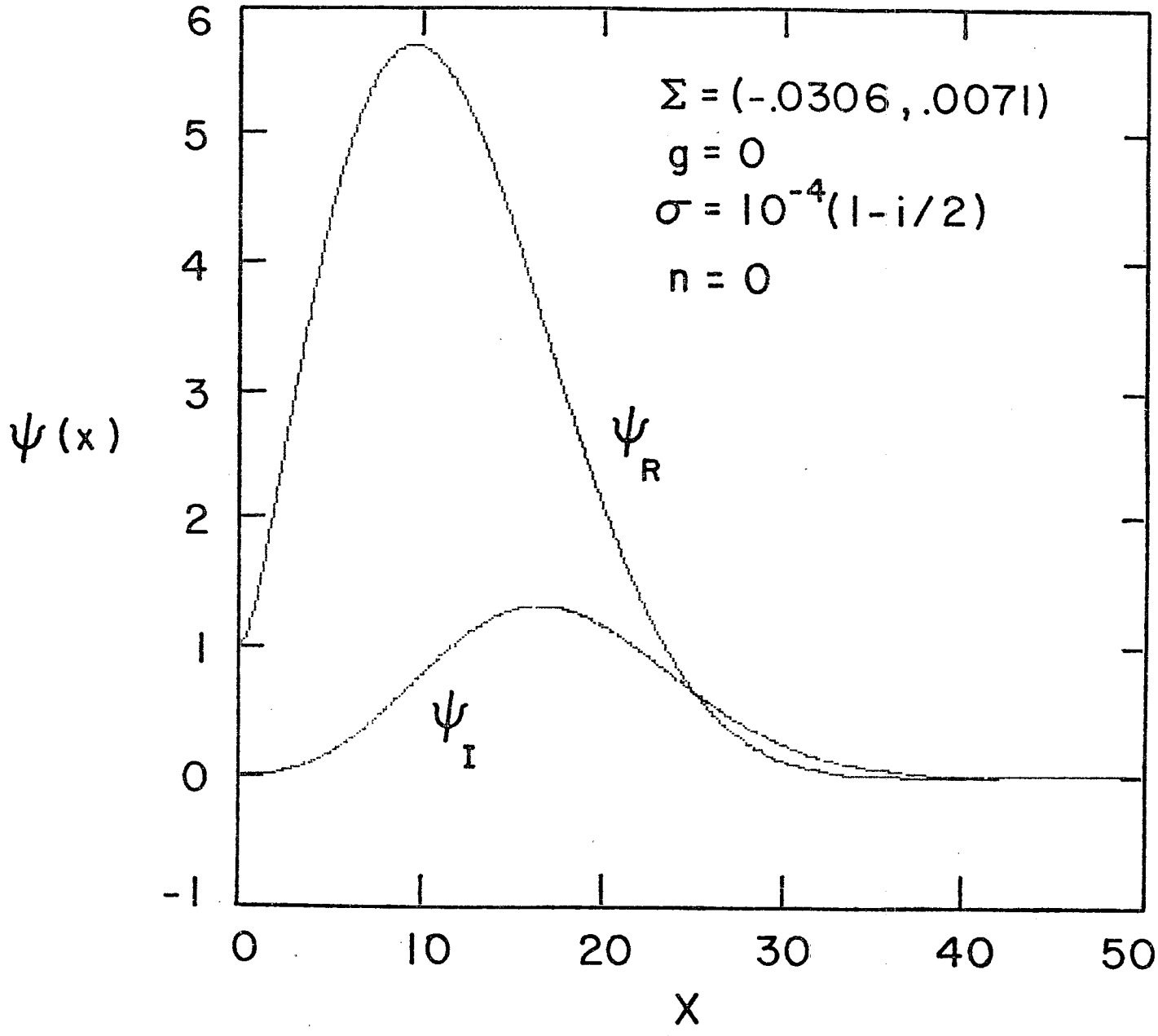

FIG. 12

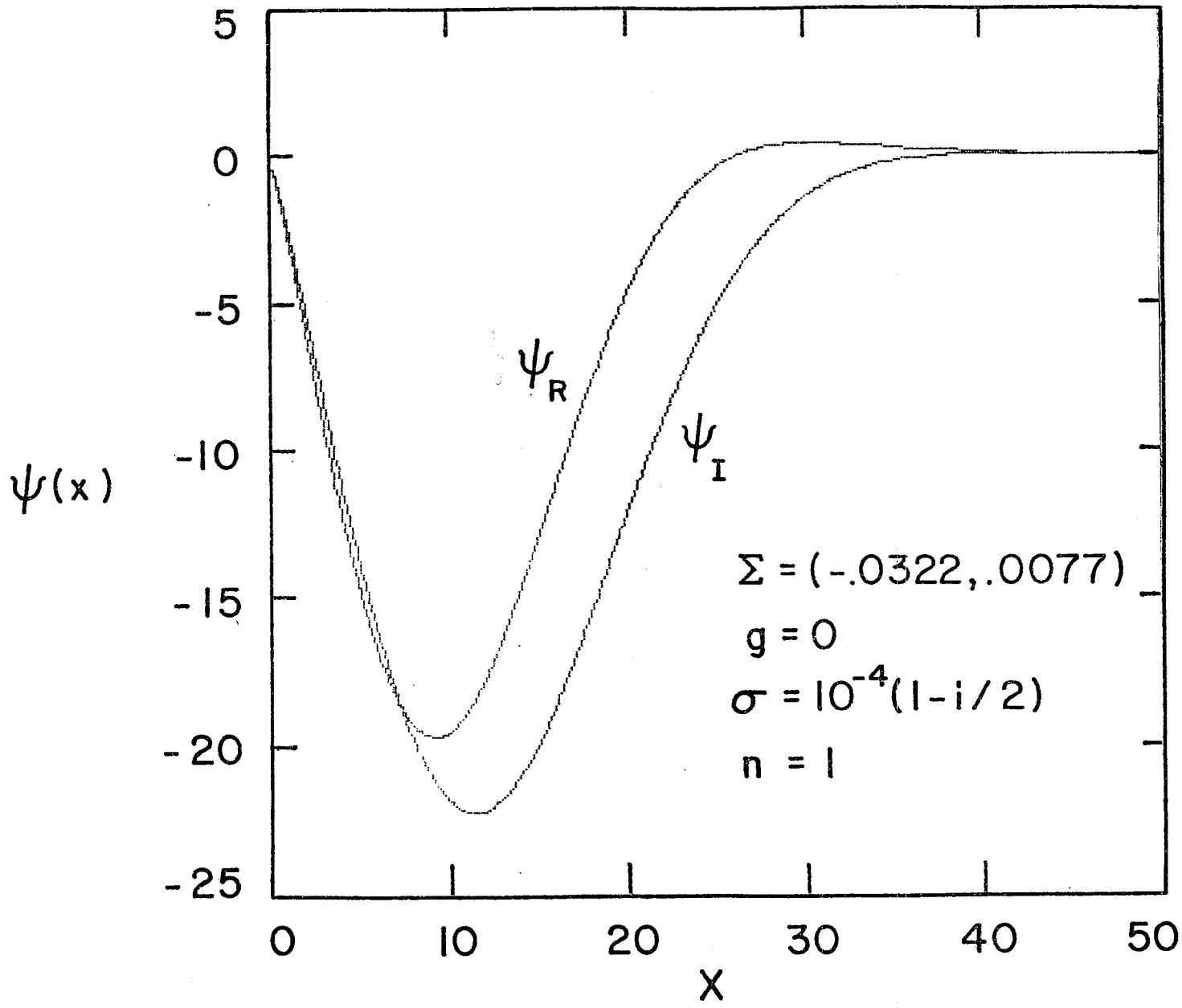

FIG. 13

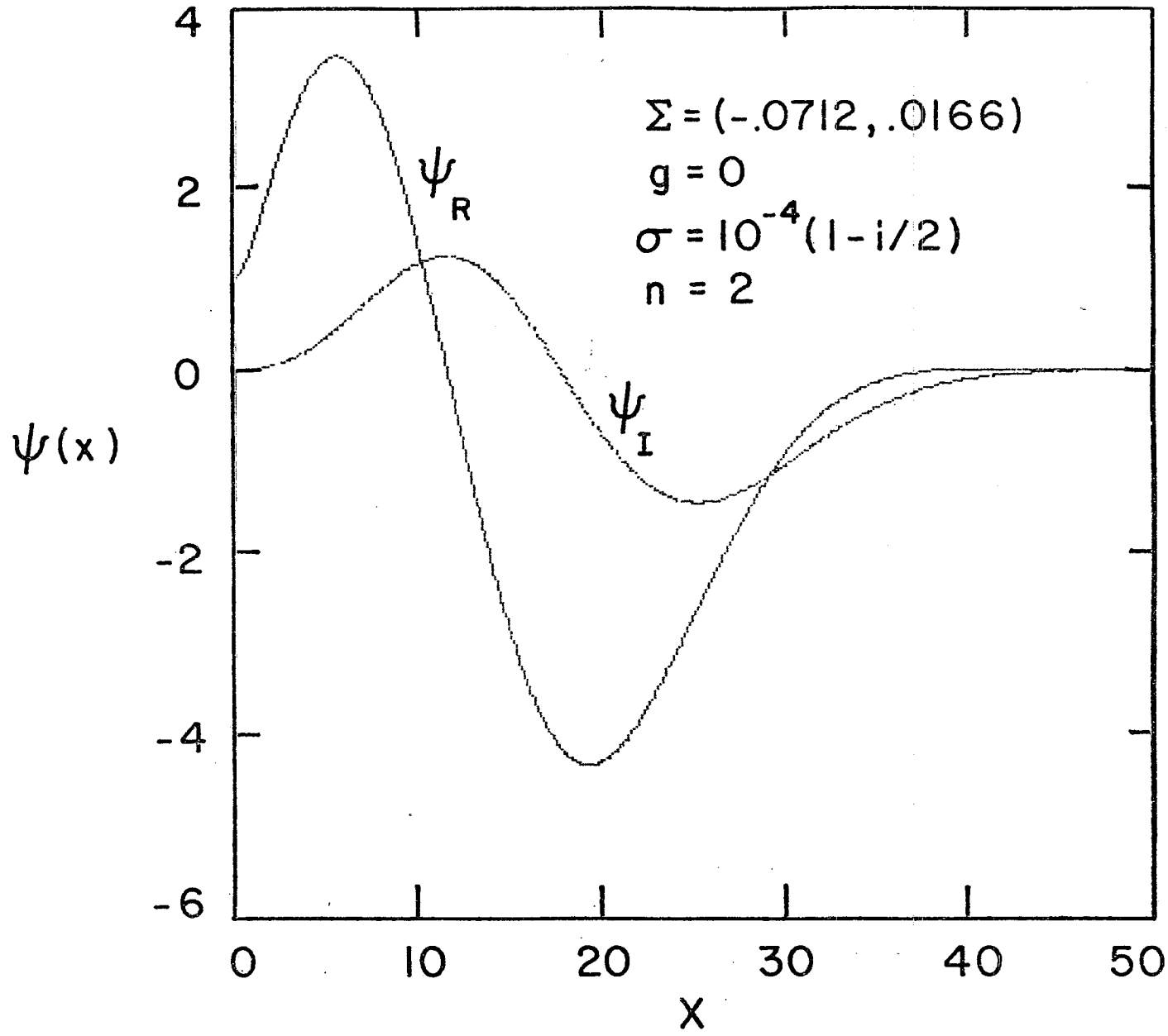

FIG. 14